MICROSCOPIC, KINETIC AND HYDRODYNAMIC HYBRID MODELS OF COLLECTIVE MOTIONS WITH CHEMOTAXIS: A NUMERICAL STUDY

MARTA MENCI, ROBERTO NATALINI, AND THIERRY PAUL

Abstract. A general class of hybrid models has been introduced recently, gathering the advantages multiscale descriptions. Concerning biological applications, the particular coupled structure fits to collective cell migrations and pattern formation scenarios. In this context, cells are modelled as discrete entities and their dynamics is given by ODEs, while the chemical signal influencing the motion is considered as a continuous signal which solves a diffusive equation. From the analytical point of view, this class of model has been proved to have a mean-field limit in the Wasserstein distance towards a system given by the coupling of a Vlasov-type equation with the chemoattractant equation. Moreover, a pressureless nonlocal Euler-type system has been derived for these models, rigorously equivalent to the Vlasov one for monokinetic initial data. In the present paper, we present a numerical study of the solutions to the Vlasov and Euler systems, exploring general settings for inital data, far from the monokinetic ones.

Contents

1. Introduction and rigorous results previously obtained

Collective motions modelling is attracting the interest of different research fields, due to the great variety of living and non-living systems exhibiting collective behaviors, see the seminal paper in [42]. Different approaches have been proposed, depending on the features models aim at reproducing and on the scale of observation. In a nutshell, all microscopic models of collective motions are based on one or more of the following elementary mechanical kind of interactions: *alignment*, see [41], [11], and references therein, *repulsion* and *attraction* [15, 37]. Concerning alignment models, one of the first and most popular model is represented by the Cucker-Smale model [11], which was originally proposed to describe the dynamics in flocks of birds, but then it was extended to cover more general phenomena, as for instance animal herding [14]. From an analytical point of view, the model and in particular the time asymptotic behaviour has been investigated in [11, 21], and then extended in different directions, see for instance [6] and [31] for a comprehensive list of references. In the biological field, collective behaviors occur in living processes involving cells dynamics, see [22, 28] for seminal review paper of the field. The main feature is that collective cells migration is also driven by a chemical stimuli, and not only by mechanical interactions among agents. On the one hand, the microscopic approach allows to model in fine details mechanical interactions among cells. On the other hand, when modelling the evolution in time of a chemical signal influencing the overall dynamics, the microscopic approach is actually not convenient, and a continuum approach, based on reaction-diffusion equation clearly better fullfill the requirement. In order to gather the advantages of microscale and macroscale approaches, a novel class of hybrid coupled models has been proposed in the last years. In particular, focusing on the family of Cucker-Smale models, in [16] a model for the morphogenesis in the zebrafish lateral line primordium was proposed. Based on the experimental data in [19, 25], the model couple a Cucker-Smale kind of interaction with other cell mechanisms (chemotaxis, attraction-repulsion, damping effects) to describe the formation of neuromasts. The description of the cell behaviour is hybrid: while particles are considered discrete entities, endowed with a radius R describing their circular shape, the chemical signal φ is supposed to be continuous and its time derivative is equal to a diffusion term, a source term depending on the position of each particle, and a degradation term The structure has been extended including stochasticity and/or further cell mechanism in [**?**, **?**, **?**]. From the analytical point of view, a simplified version of the model in [16] was proposed in [17] to allow a full analytical investigation of the asymptotic behavior, together with well posedeness results in $\mathbb{R}^2$ of the solutions. Further analytical results on generalized version of hybrid systems can be found in [29, 30, **?**].

Let us describe the class of particle systems we will handle in the present article.

Consider on $\mathbb{R}^{2dN} \ni ((x_i(t))_{i=1,\dots,N}, (v_i(t))_{i=1,\dots,N}) := (X(t), V(t))$ the following vector field

$$\left\{ \begin{array}{l} \dot{x}_i(t) = v_i \\ \dot{v}_i(t) = F_i(t, X(t), V(t)) \end{array} \right. \quad i = 1, \dots, N, \ (X(0), V(0)) = (X^{in}, V^{in}) : \tag{1}$$

where

$$F_i(t, X, V) = \frac{1}{N} \sum_{j=1}^{N} \gamma(v_i - v_j, x_i - x_j) + \eta \nabla_x \varphi^t(x_i) + F_{ext}(x_i), \tag{2}$$

Here F_{ext} is an external force, x_i, v_i are the position and velocity of the i-th cell and φ stands for a generic chemical signal produced by the cells themselves and such that the cells are attracted towards the direction where $\nabla_x \varphi$ is growing. In particular, φ satisfies the equation

$$\partial_s \varphi^s(x) = D\Delta_x \varphi - \kappa \varphi + f(x, X(s)), \ s \in [0, t], \ \varphi^{s=0} = \varphi^{in} \tag{3}$$

for some $\kappa, D, \eta \geq 0$ and function f of the form

$$f(x, X) = \frac{1}{N} \sum_{j=1}^{N} \chi(x - x_i), \quad \chi \in \mathcal{C}_c^1. \tag{4}$$

The function $\gamma : \mathbb{R}^d \times \mathbb{R}^b \to \mathbb{R} \times \mathbb{R}^d$ models the interactions among agents and it is supposed to be Lipschitz continuous[1].

Note that the case $F_{ext} = \varphi = 0$, $\gamma(y, w) = \psi(y)w$, ψ bounded Lipschitz, covers the standard case of Cucker-Smale models.

For any fixed function φ^{in} and any t, N we define the mapping $\Phi_N^t = \Phi^t$ by

$$\left\{ \begin{array}{rccl} \Phi_N^t : & \mathbb{R}^{2dN} & \longrightarrow & \mathbb{R}^{2dN} \\ & Z^{in} = (X^{in}, V^{in}) & \longrightarrow & Z(t) = (X(t), V(t)) \text{ solution of } (1, 2, 3, 4). \end{array} \right. \tag{5}$$

Note that Φ_N^t is not a flow.

In [32] a kinetic model was derived, corresponding to system $(1, 2, 3, 4)$, that is the one particle (non-linear) PDE satisfied by the first marginal[2] ρ^t of the push-froward[3] $\Phi^t \# \rho^{in}$ where $\rho^{in} \in \mathcal{P}(\mathbb{R}^{2dN})$, the space of probability measures on $\mathbb{R}^{2dN}$ and Φ_N^t is the mapping defined by (5): this is the (following non local in time) Vlasov system

$$\partial_t \rho^t + v \cdot \nabla_x \rho^t = \nabla_v (\nu(t, x, v) \rho^t), \ \rho^0 = \rho^{in} \tag{6}$$

where

$$\nu(t, x, v) = \gamma * \rho^t(x, v) + \eta \nabla_x \psi^t(x) + F_{ext}(x) \tag{7}$$

[1] through this paper we define $\mathrm{Lip}(f)$ for $f : \mathbb{R}^n \to \mathbb{R}^m, m, n \in \mathbf{N}$, as $\mathrm{Lip}(f) := \sqrt{\sum_{i=1}^{m} (\mathrm{Lip}(f_i)^2}$.

[2] definition of marginals

[3] We recall that the pushforward of a measure μ by a measurable function Φ is $\Phi \# \mu$ defined by $\int \varphi d(\Phi \# \mu) := \int (\varphi \circ \Phi) d\mu$ for every test function φ.

and ψ^s satisfies

$$\partial_s \psi^s(x) = D\Delta_x \psi - \kappa \psi^s + g(x, \rho^s), \ \psi^0 = \varphi^{in}. \tag{8}$$

with

$$g(x, \rho^s) = \int_{\mathbb{R}^{2d}} \chi(x-y)\rho^s(y,\xi)dyd\xi. \tag{9}$$

The hydrodynamic limit of Cucker-Smale models has provided up to now a large literature, whose exhaustive quotation is beyond the scope of the present paper. We refer to [6] and the large bibliography therein. In [6], the corresponding Euler equation is derived for Cucker-Smale systems with friction, using the empirical measures formalism and in a modulated energy topology. The approach and results in [32] are different: we consider generalizations of frictionless Cucker-Smale models, coupled to chemotaxis through a diffusive interaction, for large numbers N of particles and we provide explicit rates of convergences in the quadratic Wasserstein metric towards Euler type equations.

Indeed one easily sees that, in the case where ρ^{in} is monkinetic, i.e.

$$\rho^{in}(x,v) = \mu^{in}(x)\delta(v - u^{in}(x)),$$

the monokinetic form is preserved by the Vlasov equation (6) and the solution is furnished by the solution of the Euler type equation:

$$\begin{cases} \partial_t \mu^t + \nabla(u^t \mu^t) = 0 \\ \partial_t(\mu^t u^t) + \nabla(\mu^t (u^t)^{\otimes 2}) = \mu^t \int \gamma(\cdot - y, u^t(\cdot) - u^t(y))\mu^t(y)dy + \eta \mu^t \nabla \psi^t + \mu^t F \end{cases}$$

where

$$\partial_s \psi^s = D\Delta\psi - \kappa\psi + \chi * \mu^s, \ s \in [0,t], \ \Psi^0 = \varphi^{in},$$

More precisely, let the Wasserstein distance of order two between two probability measures μ, ν on $\mathbb{R}^m$ with finite second moments be defined as

$$W_2(\mu,\nu)^2 = \inf_{\gamma \in \Gamma(\mu,\nu)} \int_{\mathbb{R}^m \times \mathbb{R}^m} |x-y|^2 \gamma(dx,dy)$$

where $\Gamma(\mu,\nu)$ is the set of probability measures on $\mathbb{R}^m \times \mathbb{R}^m$ whose marginals on the two factors are μ and ν (see [43, 44]), the two main results of [32] are the following.

Theorem 1.1. *Let ρ^{in} be a compactly supported probability on $\mathbb{R}^{2dN}$, let Φ_N^t be the mapping generated by the particles system $(1,2,3,4)$ as defined by (5), and let $\tau_{\rho^{in}}$ be the function defined in* [32, Formula (41)].

Then, for any $t \geq 0$,

$$W_2\left((\Phi_N^t \# (\rho^{in})^{\otimes N})_{N;1}, \rho^t\right)^2 \leq \tau_{\rho^{in}}(t) \begin{cases} N^{-\frac{1}{2}} & d=1 \\ N^{-\frac{1}{2}} \log N & d=2 \\ N^{-\frac{1}{d}} & d>2 \end{cases}$$

where ρ^t is the solution of the Vlasov equation $(6,7,8,9)$ with initial condition ρ^{in} provided by [32, Theorem 8.1].

Moreover, let us denote by $\varphi^t_{Z^{in}}$ *the chemical density solution of* $(1,2,3,4)$ *with initial data* (Z^{in},φ^{in}) *and by* $\psi^t_{\rho^{in}}$ *the one solution of* $(6,7,8,9)$ *with initial data* (ρ^{in},φ^{in}).

Then

$$\int_{\mathbb{R}^{2dN}} \|\nabla\varphi^t_{Z^{in}} - \nabla\psi^t_{\rho^{in}}\|^2_\infty (\rho^{in})^{\otimes N}(dZ^{in}) \leq \tau_c(t) \begin{cases} N^{-\frac{1}{2}} & d=1 \\ N^{-\frac{1}{2}}\log N & d=2 \\ N^{-\frac{1}{d}} & d>2 \end{cases}$$

where τ_c *is defined below by* [32, Formula (54)].

Finally, the functions $\tau(t),\tau_c(t)$ *depend only on* t, $\mathrm{Lip}(\gamma),\mathrm{Lip}(\chi),\mathrm{Lip}(\nabla\chi)$, *and the supports of* $\Phi^t_N\#(\rho^{in})^{\otimes N}$ *and* ρ^t, *and satisfies the following estimate for all* $t\in\mathbb{R}$,

$$\tau_{\rho^{in}}(t) \leq e^{e^{Ct}},\ \tau_c(t) \leq e^{e^{C_c t}}$$

for some constants C, C_c, *depending on* $\mathrm{Lip}(\gamma),\mathrm{Lip}(\chi),\mathrm{Lip}(\nabla\chi)$ *and* $|supp(\rho^{in})|$.

Theorem 1.2. *Let* μ^t,u^t,ψ^t *be a solution to the following system*

$$\begin{cases} \partial_t\mu^t + \nabla(u^t\mu^t) = 0 \\ \partial_t(\mu^t u^t) + \nabla(\mu^t(u^t)^{\otimes 2}) = \mu^t\int\gamma(\cdot - y, u^t(\cdot) - u^t(y))\mu^t(y)dy + \eta\mu^t\nabla\psi^t + \mu^t F \\ \partial_s\psi^s = D\Delta\psi - \kappa\psi + \chi * \mu^s,\ s\in[0,t], \\ (\mu^0,u^0,\psi^0) = (\mu^{in},u^{in},\psi^{in}) \in H^s,\ s > \frac{d}{2}+1. \end{cases}$$

where $\mu^t,u^t \in C([0,t];H^s)\cap C^1([0,T];H^{s-1})$, $\psi^t \in C([0,t];H^s)\cap C^1([0,T];H^{s-2})\cap L^2(0,T;H^{s+1})$ [4].

Then $\rho^t(x,v) := \mu^t(x)\delta(v-u^t(x))$ *solves the following system*

$$\begin{cases} \partial_t\rho^t + v\cdot\nabla_x\rho^t = \nabla_v(\nu(t,x,v)\rho^t), \\ \nu(t,x,v) = \gamma(x,v) * \rho^t + \eta\nabla_x\psi^t(x) + F_{ext}(x), \\ \partial_s\psi^s(z) = D\Delta_z\psi - \kappa\psi + g(z,\rho^s),\ \psi^0 = \psi^{in}, \\ \rho^0(x,v) = \mu^{in}(x)\delta(v-u^{in}(x)). \end{cases}$$

The Euler system in Theorem 1.2 can be compared to the model of vasculogenesis in [34], which reads:

$$\begin{cases} \partial_t\mu^t + \nabla(u^t\mu^t) = 0 \\ \partial_t(\mu^t u^t) + \nabla(\mu^t(u^t)^{\otimes 2} + P(\mu^t)) = -\nu\mu^t u^t + \mu^t\nabla\psi^t \\ \partial_s\psi^s = D\Delta\psi - \kappa\psi + \chi * \mu^s,\ s\in[0,t], \end{cases}$$

with P denoting a pressure term.

The friction term can be easily introduced in our model, without changing qualitatively the results, and of course the exterior force F_{ext} can be reduced to zero.

The main difference between system (10) and the Euler system in Theorem 1.2 is the pressure term, which is replaced by the nonlocal term. This gives a derivation from microscopic setting of a the phenomenological pressure gradient non local in the density. The recent paper [40] presents a systematic study of the long-time swarming behavior of hydrodynamic Euler system accounting both alignment interaction and pressure term.

[4] We suppose this regularity because it is somehow standard for mixed hyperbolic-parabolic systems (see [27, Theorem 2.9 p. 34], one certainly could low it down.

Nevertheless our derivation is not fully satisfactory in the sense that it uses the very unsatisfactory monokinetic hypothesis on the initial data at the microscopic level. This hypothesis infers a very strong constraint on the initial data: they have to be included in an Nd submanifold of the $2Nd$ dimensional phase space, instead of having the freedom of filling the entire phase space $\mathbb{R}^{2Nd}$.

This remark suggests that the following question arises naturally: are the zeroth and first moments (in v) of the solution to the Vlasov system with general initial data ρ^{in} well approximated by the solution of the Euler system with initial data the zeroth and first moments of the initial condition ρ^{in} (see Section 3 for details)?

The numerical study of this question is one of the main objectives of the present article.

The paper is organized as follows: Section 2 review the previous numerical results established for the particle, Vlasov and Euler systmes. In Section3 we state the setting and motivations of our computation, whose precise results are contained in Section 4. We finish by Section 5 devoted to perspectives. The numerical tools used in the computations are exposed in Appendix A. Let us finish this section by recalling the three following dynamics involved in this paper, denoted by (P) for *(Particles)*, (V) for *(Vlasov)* and (E) for *(Euler)*.

$$(P)\begin{cases} \dot{x_i} = v_i,\ \dot{v_i} = F_i(t, X(t), V(t)),\ (X(0), V(0)) \in \mathbb{R}^{2dN} \\ \\ F_i(t, X, V) = \frac{1}{N}\sum_{j=1}^{N} \gamma(v_i - v_j, x_i - x_j) + \eta \nabla_x \varphi^t(x)_i + F_{ext}(x_i), \\ \\ \partial_s \varphi^s(x) = D\Delta_x \varphi - \kappa\varphi + f(x, X(s)),\ s \in [0,t],\ \varphi^0 = \varphi^{in}, \\ \\ f(x, X) = \sum_{j=1}^{N} \chi(x - x_j); \end{cases}$$

$$(V)\begin{cases} \partial_t \rho^t + v \cdot \nabla_x \rho^t = \nabla_v(\nu(t,x,v)\rho^t),\ \rho^0 = \rho^{in} \in \mathcal{P}(\mathbb{R}^{2d}) \\ \\ \nu(t,x,v) = \gamma * \rho^t(x,v) + \eta \nabla_x \psi^t(x) + F_{ext}(x), \\ \\ \partial_s \psi^s(x) = D\Delta_x \psi - \kappa\psi + g(x, \rho^s),\ \psi^0 = \varphi^{in}. \\ \\ g(x, \rho^s) = \chi * \rho^s(x). \end{cases}$$

$$(E)\begin{cases} \partial_t \mu^t + \nabla(u^t \mu^t) = 0 \\ \\ \partial_t(\mu^t u^t) + \nabla(\mu^t (u^t)^{\otimes 2}) = \mu^t \int \gamma(\cdot - y, u^t(\cdot) - u^t(y))\mu^t(y)dy + \eta \mu^t \nabla \psi^t + \mu^t F \\ \\ \partial_s \psi^s = D\Delta\psi - \kappa\psi + \chi * \mu^s,\ s \in [0,t], \end{cases}$$

2. Previous numerical results

2.1. **Particle dynamics.** The discrete-continuum hybrid system investigated in [16] correspond to (P) with $d = 1$, choosing a Cucker-Smale like interaction function

$$\gamma\left(v_i - v_j, x_i - x_j\right) = \frac{1}{\left(1 + \frac{\|x_i - x_j\|^2}{R^2}\right)^{\beta}}(v_j - v_i) \tag{10}$$

where $\beta > 0$ is the alignment parameter and $R > 0$ is the radius of the disk modelling each particle.

Initial data are given by initial position and velocity for each particle:

$$X(0) = X_0, \quad V(0) = V_0,$$

with $X(t) = (x_1(t), \ldots, x_N(t))$, $V(t) = (v_1(t), \ldots, v_N(t))$ for any $t \geq 0$, and by the initial concentration of signal, that it is assumed

$$\varphi_0 = 0. \tag{11}$$

On a linearised version of the system, authors analytically prove that the particles' aggregate exponentially converges to a state in which all agents share the same position, and the velocity converges to zero. The behavior of the full nonlinear system is investigated with a numerical approach, showing a good agreement between numerical simulations and the theoretical results on the linearised version.

2.2. **Vlasov equation.** In the present literature, several numerical methods for mean field Vlasov equations have been proposed (see [1, 7, 8] for seminal papers in the field). In particular, in [1], several stochastic Monte Carlo methods, improving classic Monte Carlo approaches, are presented, whereas in [8] deterministic splitting methods, together with semi-Lagrangian and flux balance methods, are analyzed. To the best of our knowledge, the structure of system (V), where a Vlasov-like equation is coupled with a parabolic diffusion equation, has not been investigated from a numerical point of view. For that reason, in this paper we will show numerical simulations of the novel setting.

2.3. **Euler system.** Numerical investigations on pressurless Euler systems, without chemotaxis, have been presented in [9]. Previous analytical results on this kind of system have been obtained in [5]. Authors use a Lagrangian numerical scheme to approximate the solution of one dimensional hydrodynamic systems. In particular, numerical simulations with different initial data are performed, in order to investigate regularity of the solutions, comparing global solutions and solutions exhibiting finite time blow up.

3. Setting and motivation of the present numerical study

In the present paper, we study numerically the solutions of the Vlasov and Euler systems, for various alignment models and with and without chemotaxis.

Precisely, we will study the case (10) with $\lambda = R = 1$, for various values of the parameters β and η. As we have seen in Section 2.1, parameter β leads to conditional or

unconditional flocking for the Cucker-Smale model, which can be obtained considering $\eta = 0$. Values of $\eta \neq 0$ introduces the coupling of the microscopic system to the chemical activity. Here we are interested in positive chemotactic phenomena, since cells move towards higher concentration of chemical, hence in the following we will consider $\eta > 0$.

The path

$$microscopic \longrightarrow Vlasov \longrightarrow Euler$$

corresponds to successive lacks of knowledge of the system: the meanfield limit, leading to the Vlasov equation, is obtained out of the microscopic system by averaging on all particles but one, and the passage from Vlasov to Euler retains only the moments of order zero and one in the momentum of the solution.

On the other side, the benefit of these succesive transformation is clear: the kinetic Vlasov equation deals with probabilities on finite dimensional phase spaces instead of the infinite dimensional ones of the original system, and the Euler setting describes the system by mean of densities and velocity fields on physical (configuration) spaces, that is quantities directly observable.

Finally, as explained in Section 1, the passage form Vlasov to Euler was obtained by a monokinetic hypothesis on the solution to Vlasov of the form $\rho^t(x,\xi) = \mu^t(x)\delta(\xi - u^t(x))$, shown to be rigorously equivalent for the couple (μ^t, u^t) satisfying the Euler system. If we notice that for any ρ^t of this form, one might wonder if, for more general (non monokinetic) solution to Vlasov, the quantities defined by (12) still satisfy, at least approximatively, the Euler system of equations. From a numerical point of view, this would be even more appealing for computations based on finite difference schemes, since solving a system of two PDEs, each of them in a $m-$ dimensional space, is much more economical than solving one, having dimension $2m$.

The motivation of our work is therefore threefold.

(i) show that the different features of the microscopic dynamics observed numerically in Section 2.1 are still present in the numerics of Vlasov and Euler situations.

(ii) compare, for ρ^{in} non-monokinetic, the moments of the solution to Vlasov as defined by (12) with the solution of the Euler system with initial data

$$\begin{cases} \mu^{in}(x) = \int \rho^{in}(x,\xi)d\xi \\ u^{in}(x) = \int \xi\rho^{in}(x,\xi)d\xi \end{cases} \tag{12}$$

(iii) evaluate on the settings (i) and (ii) the influence of the chemical coupling by varying the value of the parameter η from 0 to > 0.

4. Main results

In the following section we present our main numerical results. The aim of this paper is to analyze numerically some of the open problems related to generalizations of theoretical results obtained in [32]. Our aim is to present numerical insights concerning general initial data, far from the mono-kinetic one, and to investigate the role of chemical gradients at kinetic and hydrodynamic level. We restrict ourselves to observe

the behavior of the solutions of systems (P), (V) and (E) in the 1-dimensional case ($d = 1$), leaving higher dimensional cases for future research.

4.1. **Numerical Simulations of (P) and (V).** In this section we present numerical test of (V), investigating the role of alignment and chemotaxis on the overall dynamics. In each of the proposed tests we present the comparison with the particle system (P).

The schemes implemented to approximate the solution of (P) and (V) are based on finite difference approach, both for the particle/kinetic dynamics and for the parabolic equation coupled to the systems. Details of the different schemes can be found in the Appendix A.

We run the different numerical codes on a laptop equipped with an Intel Core i7-1060NG7 processor and 16 GB RAM.

4.1.1. *alignment without chemotaxis.* Negletting chemotaxis and considering only an alignment kind of interaction, systems (P) and (V) reduce to a Cucker-Smale model in a particle and kinetic regime, respectively. In the following we compare the numerical solution of the following system, hence comparing the particle and the kinetic level, respectively:

$$\begin{cases} \dot{x}_i = v_i, \\ \dot{v}_i = \dfrac{1}{N}\displaystyle\sum_{j=1}^{N} \frac{1}{(1+|x_i - x_j|^2)^\beta}(v_j - v_i) \end{cases} \tag{13}$$

$$\begin{cases} \partial_t \rho^t + v\partial_x \rho^t = \partial_v(\nu(t,x,v)\rho^t), \\ \nu(t,x,v) = \displaystyle\int_{\mathbb{R}^2} \frac{v-w}{(1+|x-y|^2)^\beta}\rho^t(y,w)dydw. \end{cases} \tag{14}$$

As already stated, numerical simulations of this kind of Vlasov equation have been already performed in [1, 7].

With respect to the previous work of the literature, here we consider a different numerical scheme, based on finite difference. In order to show that the obtained numerical solution is in good agreement with the results in [7], in this section run the numerical code starting with the same initial distribution

$$\rho^0(x,v) = \frac{1}{2\pi\sigma_x\sigma_v} e^{\frac{-x^2}{2\sigma_x^2}} \left(e^{\frac{-(v+v_0)^2}{2\sigma_v^2}} + e^{\frac{-(v-v_0)^2}{2\sigma_v^2}} \right). \tag{15}$$

with $v_0 = 3.5$, $\sigma_x = \sqrt{0.1}$, $\sigma_v = \sqrt{0.5}$.

We consider two different scenarios, depending on the value of β. In fact, as proved in the seminal paper [21], if $\beta > 0.5$ convergence to a uniform velocity is not ensured. On the contrary, if $\beta \leq 0.5$, the distribution function ρ tends to concentrate on a delta function in the velocity space and to be distributed only along the spatial dimension.

The phase space representation is obtained using the space-velocity domain $[-20, 20] \times [-5, 5]$, with $\Delta x = \Delta v = 0.1$. The time interval $[0, T] = [0, 5]$ with $\Delta t = 0.001$.

Figure 1 shows three different screenshots of a numerical simulation performed with $\beta = 0.05$. In the microscopic scale, particles' velocities tend to a common one. In a similar way, we observe that the distribution function tends to be distributed only along the spatial dimension, concentrating around the null value in the velocity space. Figure 2 shows three screenshots of a numerical simulation performed with $\beta = 0.95$. We observe that, in that case, velocities do not converge to a common one.

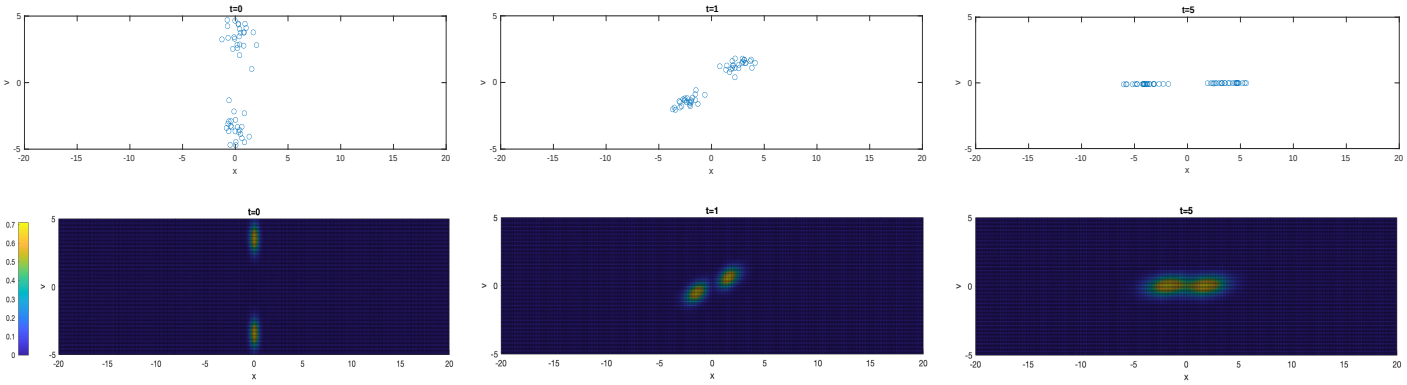

FIGURE 1. Test1: Numerical simulation of Cucker-Smale model with $\beta = 0.05$, at particle level (first line) and kinetic (second line) level.

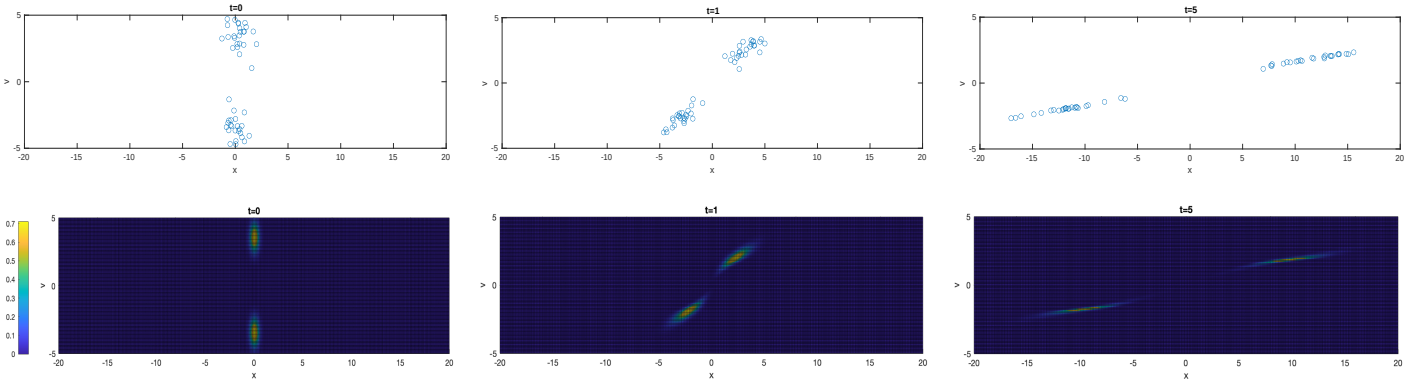

FIGURE 2. Test2: Numerical simulation of Cucker-Smale model with $\beta = 0.95$, at particle level (first line) and kinetic (second line) level.

4.1.2. *alignment with chemotaxis.* On the microscopic scale, the coupling between Cucker-Smale model and chemotaxis reads:

$$\begin{cases} \dot{x}_i = v_i, \\ \dot{v}_i = \dfrac{\lambda}{N} \displaystyle\sum_{j=1}^{N} \frac{1}{(1 + |x_i - x_j|^2)^{\beta}} (v_j - v_i) + \eta \partial_x \varphi(x_i), \\ \partial_t \varphi = D \partial_x^2 \varphi - \kappa \varphi + \displaystyle\sum_{j=1}^{N} \chi(x - x_j), \end{cases} \tag{16}$$

Let now focus on the novel coupled Vlasov-chemotaxis system, which reads as

$$
(17)\qquad \begin{cases} \partial_t \rho^t + v\partial_x \rho^t = \partial_v(\nu(t,x,v)\rho^t), \\ \nu(t,x,v) = \displaystyle\int_{\mathbb{R}^2} \frac{v-w}{(1+|x-y|^2)^\beta}\rho^t(y,w)dydw + \eta\partial_x\psi^t(x), \\ \partial_s\psi^s(x) = D\partial_x^2\psi - \kappa\psi + \displaystyle\int_{\mathbb{R}}\int_{x-R}^{x+R}\rho^s(y)dyd\xi, \end{cases}
$$

with $R, \eta > 0$.

To the best of our knowledge, there is no other works of the literature showing a numerical approach to this coupled system. The obtained results, and the comparison with the corresponding particle simulations, are not obvious and give some interesting insights.

Parameters used in the presented simulation are: $R = 10\Delta x$, $D = 1$, $\kappa = 0.01$, $\eta = 1.4$. We consider a null initial data for the chemical concentration, $\psi^0 = 0$ and the same initial distribution of the previous simulation, defined in (15).

Starting from the particle level, in [16] it has been proved that the introduction of chemotactic effects ensure convergence to a flocking state for the Cucker-Smale model, even in the cases of conditional flocking ($\beta > 0.5$). Figure 3 shows three screenshots of a numerical simulation of (17). In order to compare the behavior in the case without chemotactic interactions, we consider the same parameter setting of the simulation shown is Figure 2. Numerical evidence show that, due to the presence of a chemotactic gradient, the behavior analytically proved on the microscopic scale, is recovered also in the kinetic regime.

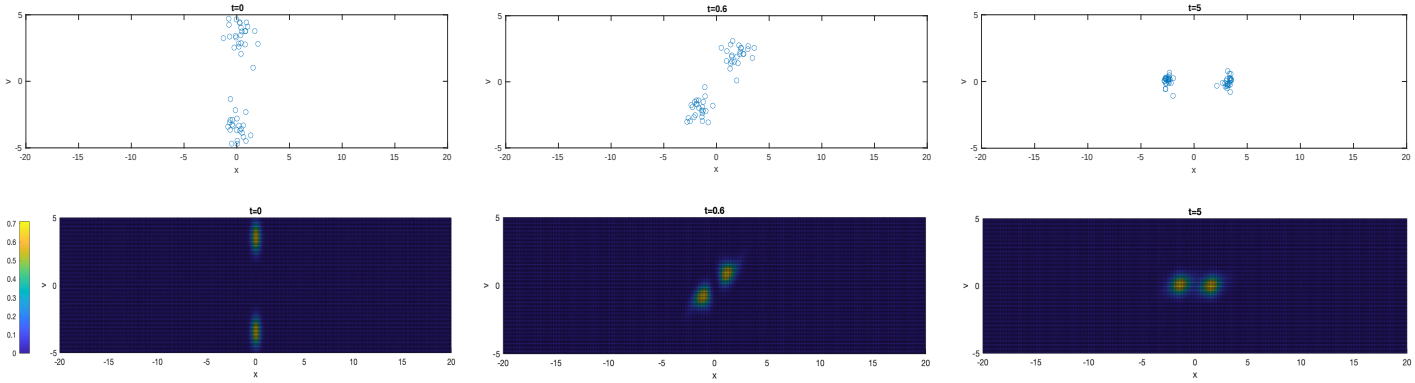

FIGURE 3. Test3: Numerical simulation of Cucker-Smale model with chemotaxis at particle level (first line) and kinetic (second line) level, with $\beta = 0.95$ and $\eta = 1.4$.

4.1.3. *chemotaxis without alignment.* In order to investigate the role of the alignment term, we here show the result of a numerical simulation in the case of a pure chemotactic kind of interaction. We consider system (17), negletting the alignment interactions, hence the integral term. The evolution in time of the density is influenced by the gradient of the chemicals. At particle level, the absence of alignment results in an oscillatory behavior of the particles around the center of mass. Figure 4 shows three screenshots of a numerical simulation, at three different time instant. The initial condition is the same of the previous tests. We observe that the oscillating behavior observed in particle dynamics, is reproduced even at the kinetic level.

$$
\begin{cases}
\partial_t \rho^t + v\partial_x \rho^t = \partial_v(\nu(t,x,v)\rho^t), \\
\nu(t,x,v) = \eta \partial_x \psi^t(x), \\
\partial_s \psi^s(x) = D\partial_x^2 \psi - \kappa\psi + \displaystyle\int_{\mathbb{R}} \int_{x-R}^{x+R} \rho^s(y) dy d\xi,
\end{cases} \tag{18}
$$

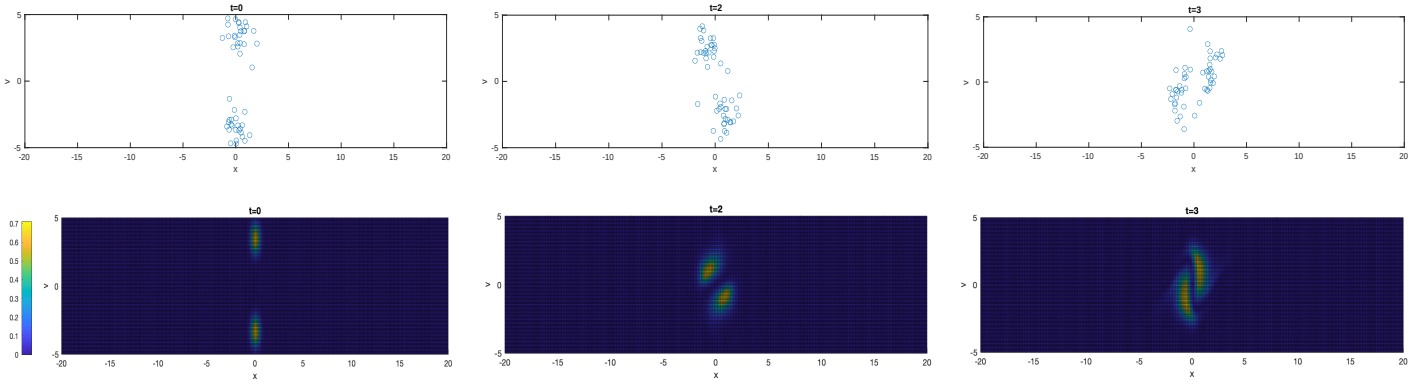

FIGURE 4. Test 4: Numerical simulation of (18) with $\eta = 1.4$

4.2. **Numerical Simulations of (E).** We present some numerical simulations of (E), both in absence and in presence of chemotaxis. This model writes as a hyperbolic-parabolic non local system for macroscopic quantities: density, momentum and concentration of a chemoattractant.

$$
\begin{cases}
\partial_t \mu^t + \partial(u^t \mu^t) = 0 \\
\partial_t(\mu^t u^t) + \partial(\mu^t (u^t)^2) = \mu^t \int \gamma(\cdot - y, u^t(\cdot) - u^t(y))\mu^t(y) dy \\
\qquad\qquad\qquad\qquad + \eta \mu^t \partial_x \psi^t \\
\partial_s \psi^s = D\partial_x^2 \psi - \kappa\psi + \displaystyle\int_{x-R}^{x+R} \mu^s(y) dy, \ \ s \in [0,t].
\end{cases} \tag{19}
$$

As for system (V), we will investigated, from a numerical viewpoint, the effect of chemotaxis on the solution, comparing two cases: $\eta = 0$ and $\eta \neq 0$. The final aim is in fact to gain some numerical insights on the role of chemotaxis on the solution of pressureless Euler system.

4.2.1. *without chemotaxis: finite time blow up of solution.* As a first step, we neglect chemotaxis, and system (19) reduces to a 1-dimensional pressureless Euler-alignment system:

$$\begin{cases} \partial_t \mu^t + \partial(u^t \mu^t) = 0 \\ \partial_t(\mu^t u^t) + \partial(\mu^t (u^t)^2) = \mu^t \int \gamma(\cdot - y, u^t(y) - u^t(\cdot))\mu^t(y)dy \end{cases} \tag{20}$$

Analytical results and numerical insights on the stability of flock solutions for this system can be found in [10, 9]. In [10], authors distinguish between *supercritical* and *subcritical region*: initial data lying in the *supercritical region* lead to blow up of the solution, whereas starting with data in the *subrcritical region* global existence of the solution is ensured. In [9] different numerical simulations, with data lying in both regions, are performed. In particular, numerical simulations are performed in the spatial domain $[-0.75, 0.75]$ discretized with 200 uniformly distributed points, choosing initial data

$$\mu^0(x) = c_1 \cos\left(\frac{\pi x}{1.5}\right), \tag{21}$$

$$u^0(x) = -c_2 \sin\left(\frac{\pi x}{1.5}\right) \tag{22}$$

where c_1 is the normalization factor, and $c_2 > 0$ is varied in the different simulations, in order to show the behavior of the solutions.

With respect to the Lagrangian numerical scheme adopted in the previous paper, we here implement a finite difference numerical scheme based on a Relaxation scheme for Euler system [2]. Starting with the same initial data, the obtained results are in good agreement with the ones in [9].

Figure 5 (first line) shows the density and velocity profile obtained for $c = 0.2$ for three different time instants. This case correspond to initial data in the subcritical region, and the convergence of the velocity to zero correspond to the expected global consensus. On the contrary, figure 5 (second line) shows the density and velocity profile obtained for $c = 0.5$, which correspond to initial data in the supercritical region. The velocity profiles, with derivative getting larger negative at the origin as time goes, reflect in high values of the density solution, which almost cannot be solve numerically after $t \approx 3$.

The obtained results represent the starting point for some numerical investigations, concerning the effect of the introduction of a chemotactic effect and a damping term.

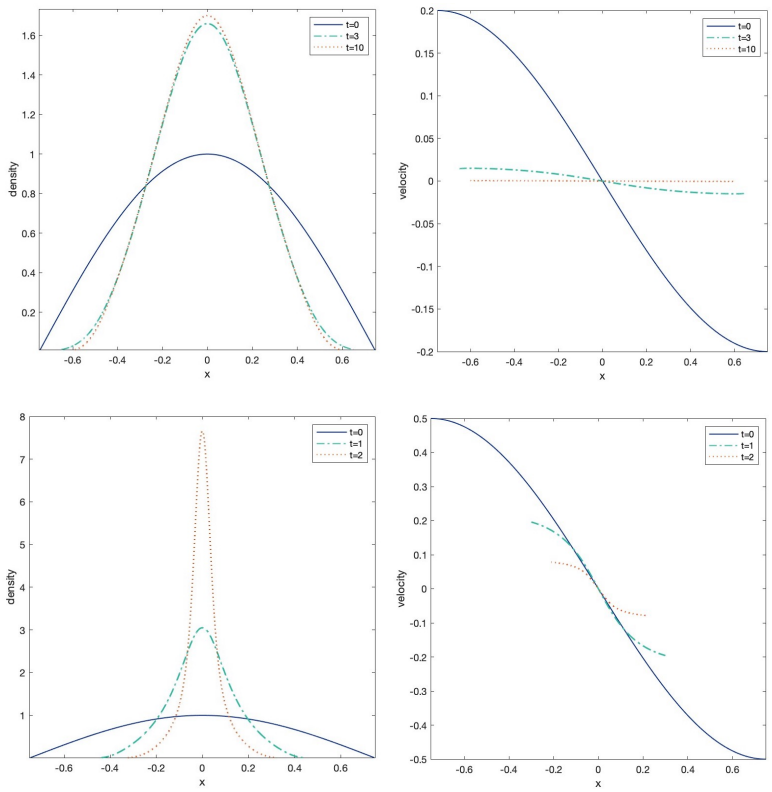

FIGURE 5. Test5: Numerical simulation of (20)-(22) for $c_2 = 0.2$ (first line) and $c_2 = 0.5$ (second line).

4.2.2. *with chemotaxis and/or damping.* Let now consider the full Euler-coupled system in (19), also adding a possible damping term:

$$
\begin{cases}
\partial_t \mu^t + \partial_x(u^t \mu^t) = 0 \\
\partial_t(\mu^t u^t) + \partial_x(\mu^t (u^t)^2) = \mu^t \int \gamma(\cdot - y, u^t(\cdot) - u^t(y))\mu^t(y)dy \\
\qquad\qquad\qquad\qquad +\eta \mu^t \partial_x \psi^t - \alpha \mu^t u^t \\
\partial_s \psi^s = D\partial_x^2 \psi - \kappa \psi + \displaystyle\int_{x-R}^{x+R} \mu^s(y)dy, \ \ s \in [0,t].
\end{cases} \tag{23}
$$

where η and α are nonnegative constants regulating the chemotactic and the damping influence, respectively.

Concerning the numerical scheme, we put in implicit the damping term in the equation of the momentum, and approximate the solution of the parabolic equation as already explained.

Figure 6 shows the results of three different tests. First, we simulated the setting with data in the subcritical region already seen ($c_2 = 0.2$, $\alpha = 0$) adding the chemical influence ($\eta = 1$). Numerical evidence show that the global consensus is still preserved, and the addiction of a chemotactic influence enhance the effect. In the other test

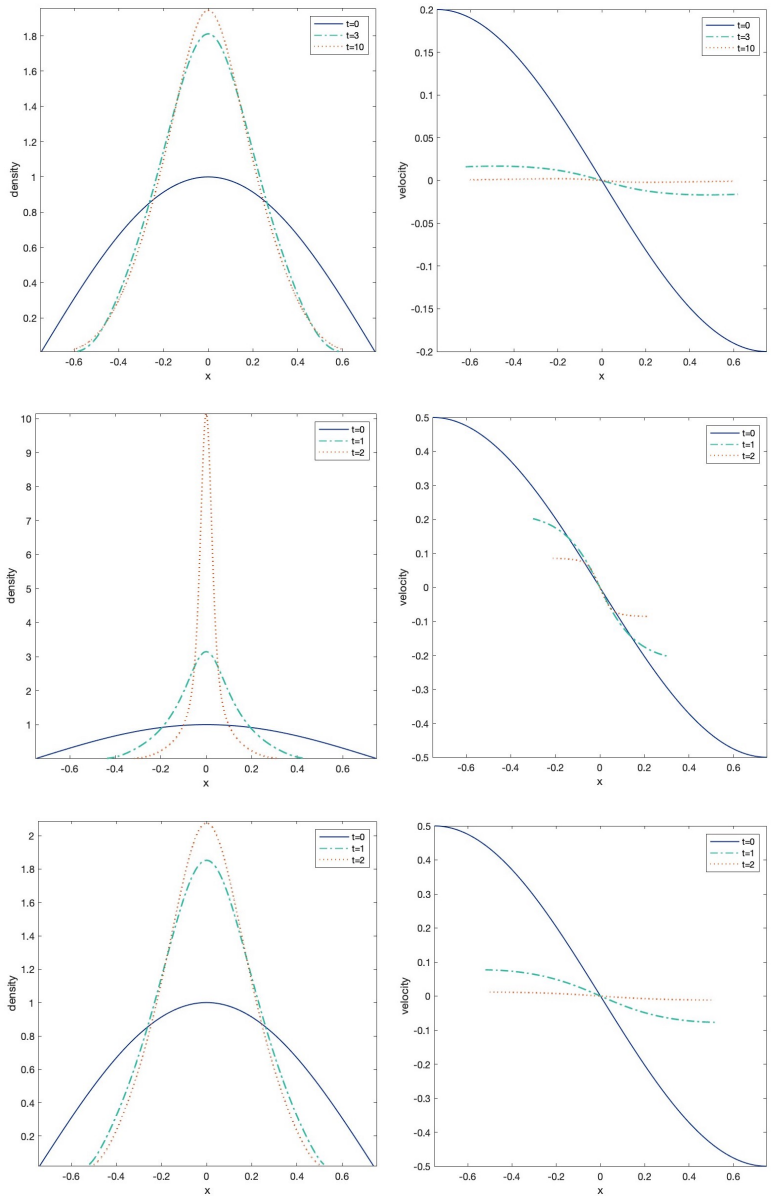

FIGURE 6. Test6: Numerical simulation of (23) with initial condition (21),(22). First line: $c_2 = 0.2$, $\eta = 1$, $\alpha = 0$; second line: $c_2 = 0.5$, $\eta = 1$, $\alpha = 0$; third line $c_2 = 0.5$, $\eta = 0$, $\alpha = 1$.

(Figure 6, second and third lines) we investigate the role of chemotaxis and damping in suppressing the blow-up phenomena ($c_2 = 0.5$). Numerical evidence (Figure 6, second line) show that a pure chemotactic effect ($\eta = 1$, $\alpha = 0$) enhance the blow-up phenomena: density value at the origin is higher than the case without chemotaxis, and the derivative of the velocity is sharper. The presence of a damping term seems to play the crucial role, as shown in (Figure 6, third line). Here, the blow up exhibited in the same setting without damping (see Fig. 5) is recovered: velocity converges to zero and global consensus is reached.

4.3. **Numerical comparison between (V) and (E).** We introduce the following notation for the zero-th and first order moments of the solution ρ, respectively

$$\nu_0^t(x) = \int \rho^t(x,\xi)d\xi, \tag{24}$$

$$\nu_1^t(x) = \int \xi\rho^t(x,\xi)d\xi \tag{25}$$

In the following we compare, for different choices of ρ^0 involving different scenarios, ranging from almost monokinetic to largely non-monokinetic, the moments of the solution to Vlasov with the solution of the Euler system with initial data

$$\begin{cases} \mu^0(x) = \nu_0^0(x) \\ \\ Q^0(x) = \nu_1^0(x) \end{cases} \tag{26}$$

where $Q^t := \mu^t u^t$ denotes the momentum for any $t \geq 0$.

We now compute initial data (μ^0, Q^0) for the Euler system as defined in (26), and we numerically solve (E). As in the previous simulations, we will consider two scenarios: without and with chemotaxis. Our aim is to compare the behavior of ν_0^t and ν_1^t with density μ^t, and momentum Q^t, in order to investigate, from a numerical view point, the case of non monokinetic initial data.

4.3.1. *Monokinetic initial data.* We recall that analytical results obtained in [32] ensure a complete correspondence between Vlasov moments and Euler solutions, in case of monokinetic initial data. As a preliminary test, we consider a numerical approximation of the monokinetic initial data, choosing a gaussian distribution with low value of σ_v parameter. In greater detail, in this test we choose

$$\rho^0(x,v) = \frac{1}{2\pi\sigma_x\sigma_v} e^{\frac{-(x-x_0)^2}{2\sigma_x^2} + \frac{-(v-v_0)^2}{2\sigma_v^2}}. \tag{27}$$

with $x_0 = -2$, $v_0 = 1.5$, $\sigma_x = \sqrt{0.2}$, $\sigma_v = \sqrt{0.001}$. Clearly, even choosing a small value for σ_v, we are considering an approximation of the monokinetic case, and we do not expect a full correspondence with the analytical results on this case. We choose initial conditions for (E) are defined as in (26), and run the simulations for the case without and with chemotaxis.

Figure 7 shows the plot of ρ^0 in the phase space, and the profile of initial data for (E) (blue dotted line), which are defined in (26) and correspond to Vlasov moments (cyan line) . Figure 8 shows the behavior, at the same time instant $t = 2$, of ν_0^t and ν_1^t together with μ^t and Q^t respectively, both without (first line) and with chemotactic effect (second and third line). The evolution of Vlasov dynamics preserve the monokinetic (approximated) initial structure, and Vlasov moments and Euler solutions are in good agreement when simulating the case without chemotaxis. Numerical evidence

show that adding chemotaxis, the approximated monokinetic-like structure is not preserved for long time. As already observed at particle level, the presence of a chemical gradient influencing the dynamics tends to concentrate the density profile in the same point, and to asymptotically let the velocities converge to zero. This can be seen in the phase space (first column, second line). Moreover, introducing also a damping term, the momentum tends to zero faster (third line). Focusing on the Vlasov moments, we observe that as soon as the monokinetic structure is lost, the agreement between Vlasov moments and Euler solution is worse. In particular we observe a blow-up of the density profile. In conclusion, the monokinetic property seems to play a crucial role. For that reason we exploit with several tests the case of largely non monokinetic initial data.

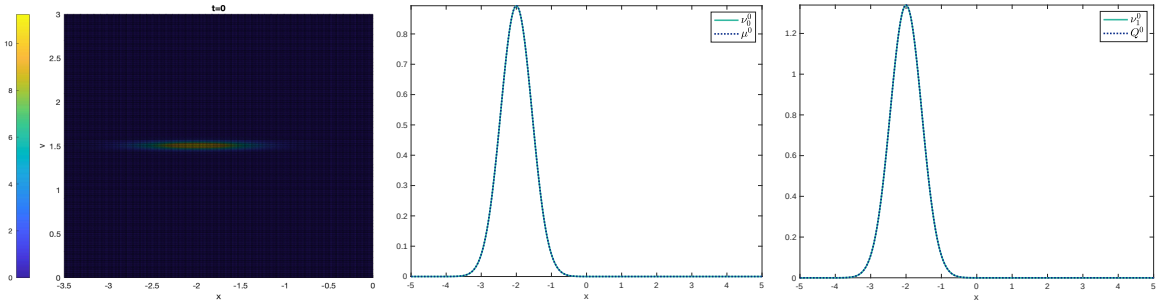

FIGURE 7. Test 7: Initial condition

4.3.2. *Non monokinetic initial data.* In section 4.1 we already considered a non monokinetic initial data for Vlasov equation, see (15). In particular, Test 2 and Test 3 exploit, at kinetic level, the case without and with chemotaxis. We complete our multiscale analysis, choosing as initial data for Euler equation (26) with initial distribution function as in (15). Figure 9 shows initial conditions for the following Test 8 and Test 9.

In Test8 we compare the moments ν_0^t and ν_1^t of the solution of (14)-(15) with the solution of system (20) with initial conditions (26). Since $u^0(x) = 0$, the velocity u^t remains zero, being a stationary solution for Euler system. On the contrary, the first order moment profile shows the separation due to the effect of speeds. As shown in Figure 10, there is no agreement between Vlasov moments and Euler solutions. This in due to the fact that, in Euler system, the role of v as a variable is lost.

Let now solve (23), with $\eta = 1.4$. Figure 11 shows three different snapshots of the numerical simulation performed. At the beginning, we observe that the spreading of the speed in the density, solution of Vlasov equation, is stronger than the chemistry, and two separate peaks appear. With respect to the previous case, the presence of the chemotactic gradient prevent the separation observed for longer time, leading to the convergence to a unique bump. Concerning the first order moment (Vlasov) and the momentum (Euler), at the beginning they are both null. Due to the presence of chemicals, $u^t(x) = 0$ is no longer a stationary solution for Euler but asymptotically in time

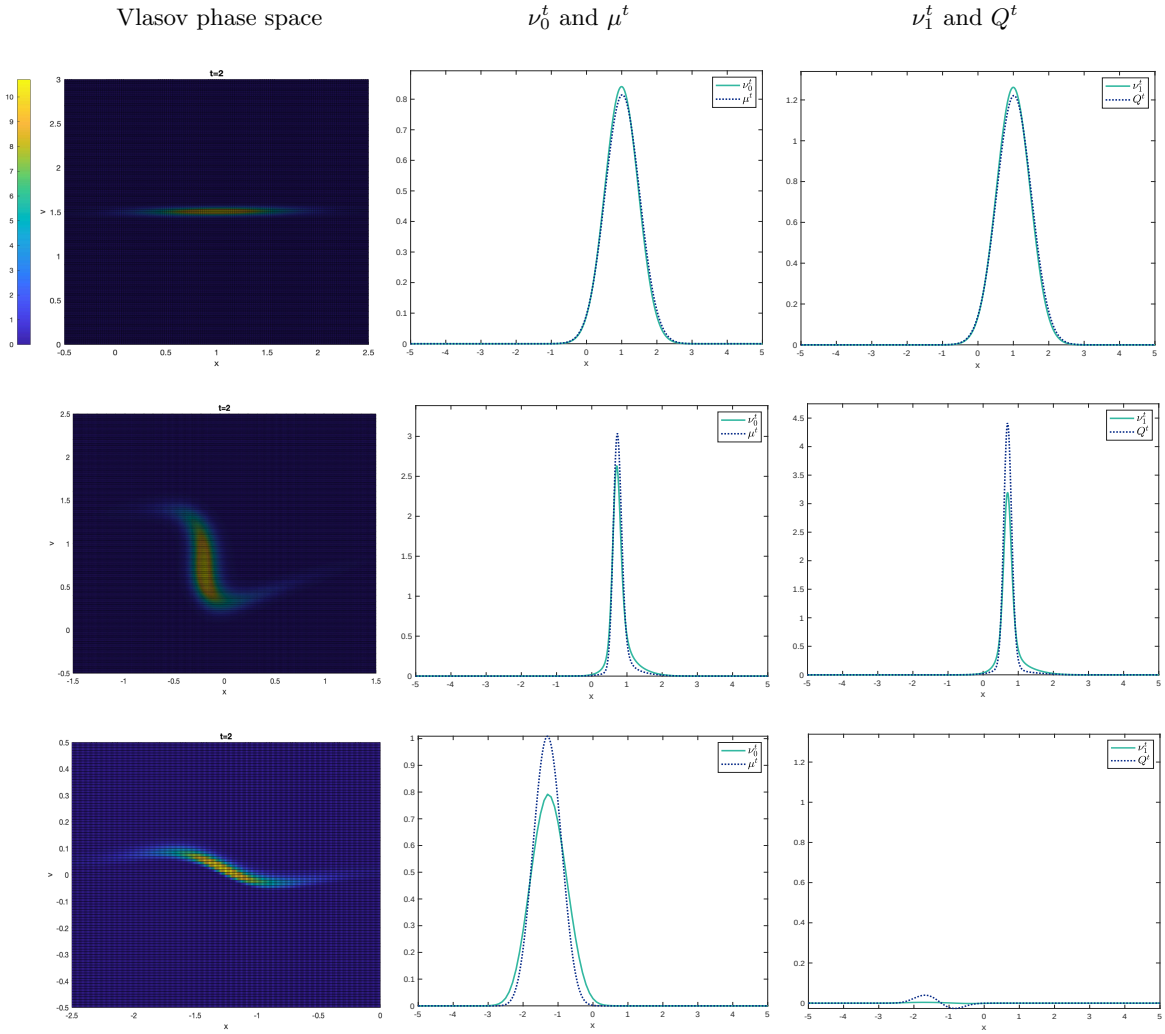

FIGURE 8. Test 7: approximation of monokinetic initial data. Comparison between zero-th order moment of the solution of (V) and μ^t (second column), first order moment of the solution of (V) and Q^t (third column): without chemotaxis (first line: $\eta = 0$, $\alpha = 0$ at $t = 2$), with chemotaxis (second line: $\eta = 0.2$, $\alpha = 0$ at $t = 2$), with chemotaxis and damping (third line: $\eta = 0.2$, $\alpha = 2$ at $t = 2$).

moment and momentum decay to zero, as seen at particle level, and the convergence is faster adding the damping term.

We observe that, as time grows, the agreement between Vlasov moments and Euler solution is quite good especially for the density. One could think that chemical plays the crucial role. For that reason we consider the scenario without alignment, where only a chemotactic effect rules the dynamics. At kinetic level, we have already discussed the results (see Test 4 and Figure 4). Figure 12 shows the results of the comparison. We observe that the agreement between Vlasov moments and solutions of Euler is not recovered. The zero-th order moment shows the observed oscillations, with two bumps separating and merging, as reflecting by the sign of the first-order moment. The oscillating behavior is not reproduced in the solution of Euler, where the speed variable does not play a role as in Vlasov. To conclude, numerical evidence shows that, starting with a non monokinetic initial data exhibited in Figure 9 the combined effect of alignment kind of interaction and chemotaxis asymptotically leads to a good

agreement. Numerical evidence seems to suggest that the combination of alignment and chemotaxis play a crucial role in the comparison among the two scales.

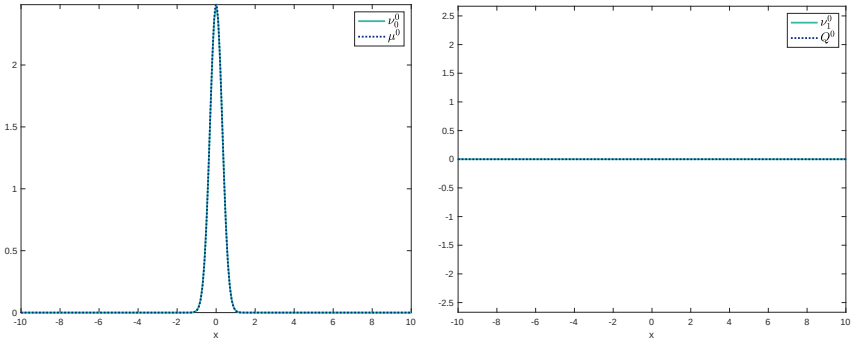

FIGURE 9. Test8, Test9, Test10: Initial condition

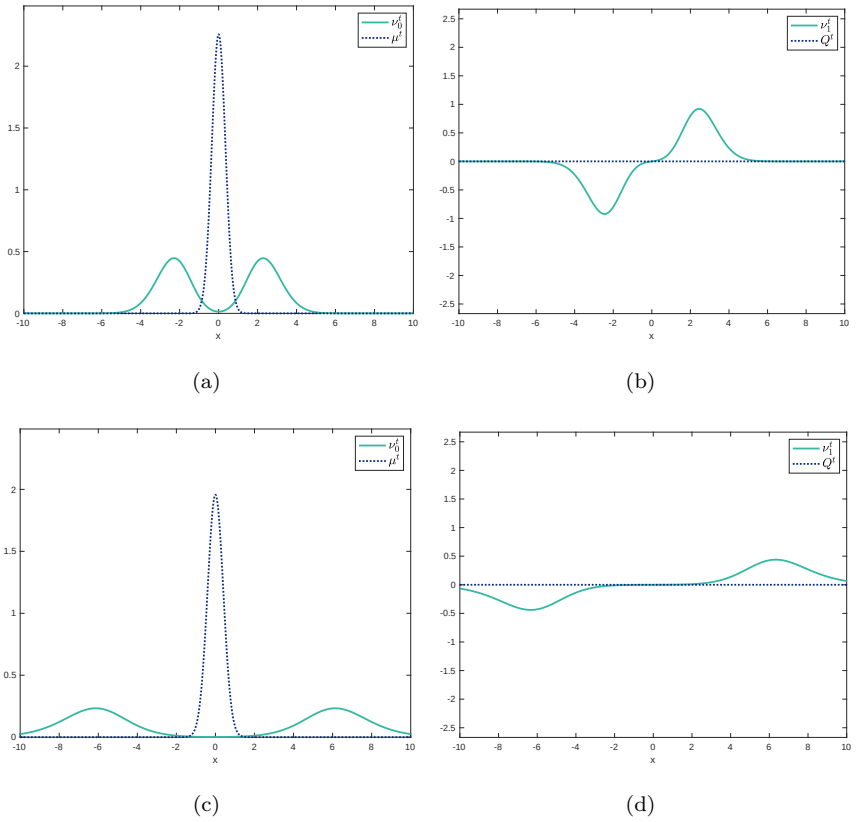

FIGURE 10. Test 8: Comparison between zero-th order moment of the solution of (V) and μ^t, first order moment of the solution of (V) and Q^t at a),b) $t = 1$, c),d) $t = 3$. Here $\eta = 0$ (no chemotaxis), $\alpha = 0$.

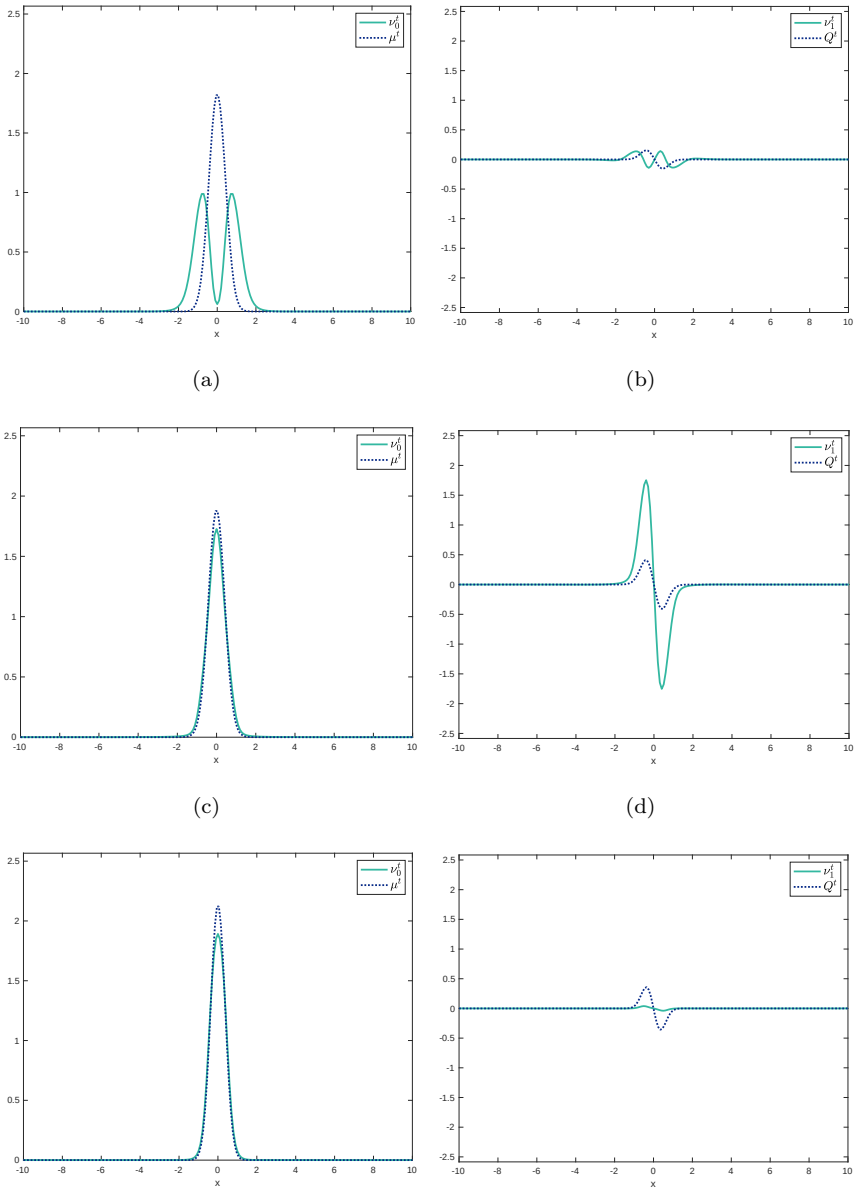

FIGURE 11. Test 9: Comparison between zero-th order moment of the solution of (V) and μ^t, first order moment of the solution of (V) and Q^t at a),b) $t = 0.5$, c),d) $t = 1$, e),f) $t = 7$. Here $\eta = 1.4$, $\alpha = 0$.

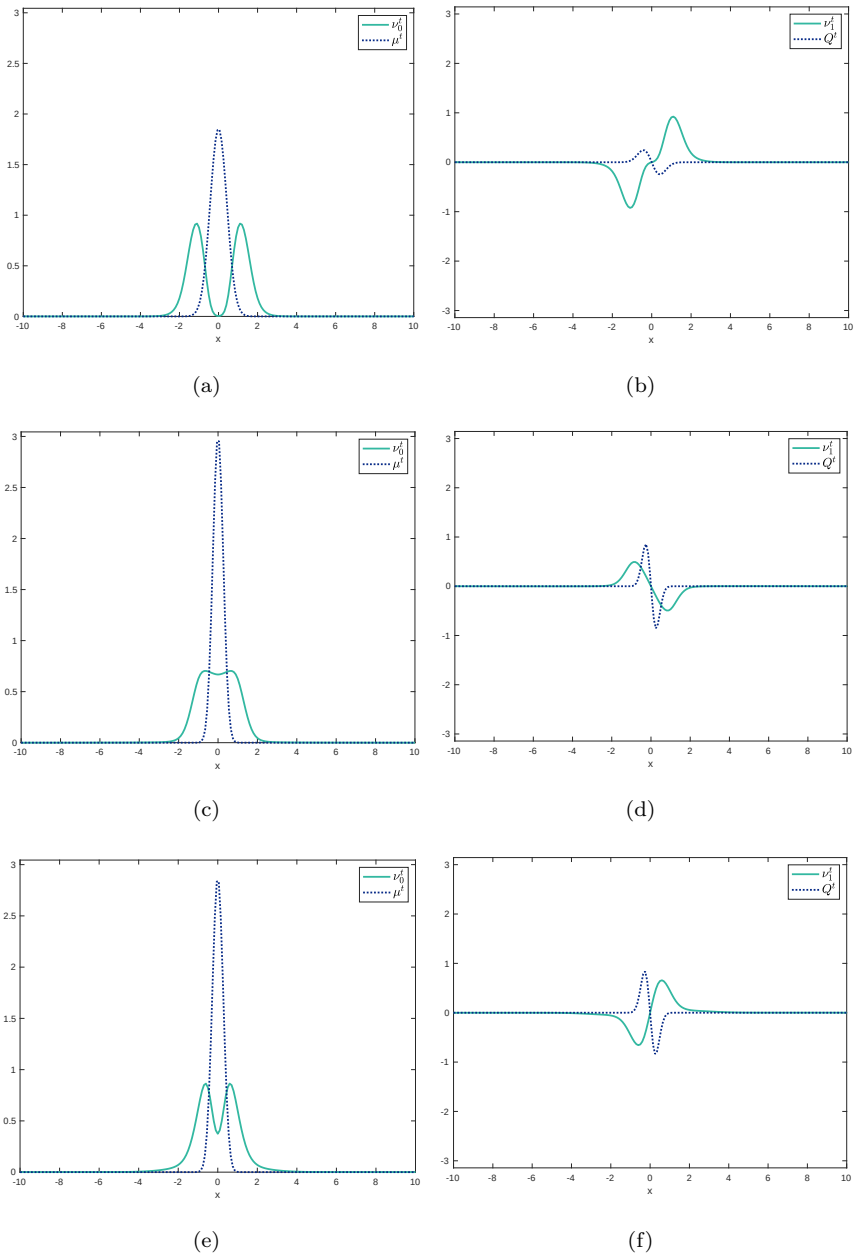

FIGURE 12. Test 10: Comparison between zero-th order moment of the solution of (V) and μ^t, first order moment of the solution of (V) and Q^t at a),b) $t = 0.5$, c),d) $t = 2$, e),f) $t = 3$. Here $\eta = 3.4$, $\alpha = 0$ and the integral term in (E) is negletted.

5. Comments and perspectives

Let us remind the link between the particle system (1)-(4) and the corresponding Vlasov system (6)-(9). One first consider a 'chaotic" probability density

$$\rho_N^{in} := (\rho^{in})^{\otimes N} \tag{28}$$

on $\mathbb{R}^{2dN}$, ρ^{in} being a probability density on $\mathbb{R}^{2d}$. The meaning of $\rho_N^{in}(X_N, Z_N) = \rho_N(x_1, \dots, x_N; v_1, \dots, v_N)$ is clear : it is the probability that every particle indexed by $i = 1, \dots, N$ is at the position x_i and has the velocity v_i. The hypothesis (28) means that all particle are in the same initial "state", namely have the same probability distribution in phase space (chaotic assumption). To ρ_N^{in} we associate for any time t its pushforward

$$\rho_N^t := \Phi^t \# \rho^{in} \tag{29}$$

by the flow Φ_N^t defined by (5), strictly tight to the particle system. Note that if Φ_N^t defined by (5), i.e. the particle system (1)-(4), define ρ_N^t, the inverse is also true: the knowledge of ρ_N^t for every ρ_N^{in} determines Φ_N^t. Once again the link between the particle and the Vlasov systems works the following way: to the N-particle distribution$\rho_N^t = \Phi^t \#(\rho^{in})^{\otimes N}$ we associated its first marginal $(\rho_N^t)_{N;1}$ whose definition is recalled in the footnote 1, proved to tend as $N \to \infty$ to the solution of the one-particle Vlasov system (6)-(9) with initial data ρ^{in}. Of course, at time $t = 0$ the consistency is total, even at N fixed, since for any integer N, tautologically

$$(\rho_N^{t=0})_{N;1} = ((\rho^{in})^{\otimes N})_{N;1} = \rho^{in}, \tag{30}$$

so that the initial probability distribution for the Vlasov equation is nothing but the common initial probability distribution of each particle for the particle system . But (30) is not anymore valid for $t > 0$ since the interaction between particle breaks the factorization property (28): $(\rho_N^t)_{N;1} \neq= \rho^t$ but, as $N \to \infty$, $(\rho_N^t)_{N;1} \to \rho^t$. To put it in a nutshell:

averaging a particle system over all particles but one leads when the number of particle diverges to a nonlinear one-particle conservation law driven by the vector field obtained by averaging the original one by the solution itself.

This last aphorism shows clearly that the link between particle systems and thier corresponding Vlasov' s noes is subtle, more subtle according to us `(us?)` than a simple discretization of a PDE. It correspond to a somehow mysterious, at lesat non trivial, intertwining property between two averaging process: a first one on moving $(N-1)$ particle and a second one on the generator of a 1-particle conservation law. Although this propagator is related to the original particle system, the fact that this intertwining holds true is not obvious, and, more than that, it seems to us that the phenomenological comparison of the solution of a particle system and its associated Vlasov one - a fortiori when one adds the Euler one - is an issue, specially considering the fact that different computational complexities are involved. This is what we believe is the interest of our work.

Indeed in this paper we investigated numerically three different levels of descriptions of several models of dynamics of interacting cells subject to chemotaxis: the microscopic particle one (P), introduced in [17], the phase space (position-momentum) density Vlasov type description (V) and the physical space density-velocity field Euler type description (E), these two last ones having been introduced and analytically studied in [32].

Although each passage between the three levels consists in loosing some information - averaging on every but one particle and letting the number of particles diverge for $(M) \to (V)$ and taking only zeroth and first moments in velocity for $(V) \to (E)$ - we show that in many situations the most striking features of the particle level (P) - conditional and non conditional alignment, chemo-attraction - are preserved by passing from the paradigm of N particles to the one of Vlasov at $N \to \infty$. Obviously this seems to us an interesting result as solving a $2D$ PDE is numerically more easy than a truly infinite number on ODE.

For the passage $(V) \to (E)$, realizing an even more economical numerical gain as passing from a $2D$ PDE to a system of two $1D$ PDEs, the situation is more diverse: the fidelity of Euler versus Vlasov is always increased by the presence of the chemical interaction (in fact the mixing of the alignment and chemotaxis), leading to positive results event for systems not presenting the condition of a corresponding rigorous mathematical result. In this framework the sensitivity to the form of the initial condition remains a serious issue.

The first perspectives following this work will be the case of two dimensional setting for the particle system, that is $4D$ Vlasov equation, and to inquire the (possibly very) long time behavior of all these correlations between three different scales description of biological systems.

Appendix A. Numerical schemes

In the following we detail the numerical schemes used for the numerical simulations of the different equations.

Particle level: numerical scheme for (P)

For the ODE part of the coupled system, we implemented the well-known implicit Euler method, whereas the chemotaxis equation is discretized computing at each time the value of the solution on grid point discretizing the spatial domain.

We consider the simulation time interval $[0, T]$, for some $T > 0$, divided into subintervals of same size Δt, assuming that T is a multiple of Δt to avoid rounding. We define $n_T := \frac{T}{\Delta t} \in \mathbb{N}$, and denote the time grid points as $\{t^0, \ldots, t^{n_T}\}$. Finally, (x_i^k, v_i^k) denote approximations of position and velocity of agent i at time t^k, for any $i = 1, ..., N$, $k = 1, ..., n_T$ starting with initial condition (x_i^0, v_i^0).

Focusing on the chemotaxis equation, we eliminate the stiff degradation term performing the classical exponential transformation $\varphi^s(x) = e^{-\kappa s}u^s(x)$, where u solves

$$\partial_t u = D\partial_x^2 u + e^{\kappa t}\sum_{j=1}^{N}\chi(x - x_j), \tag{31}$$

We approximate the solution by means of a second order centered finite differences method in space and a classical explicit-implicit Crank-Nicholson integration in time, assuming periodic boundary conditions. The computational domain $\Omega \times [0, T]$, for some $\Omega \subset \mathbb{R}$, is divided in cells of side $\Delta x \times \Delta t$, where Δx denotes the space step, and the time step is the same used for the ODE part. We denote with n_Ω the total number of the spatial grid points $\{\omega_0, \dots, \omega_{n_\Omega}\}$. In greater details, denoting with u_l^k the approximation of u at the grid point (y_l, t^k), the numerical scheme reads

$$\begin{aligned}\frac{u_l^{k+1} - u_l^k}{\Delta t} = D\frac{u_{l-1}^k - 2u_l^k + u_{l+1}^k}{(\Delta x)^2} &+ \frac{1}{2}e^{\kappa(k+1)\Delta t}\sum_{j=1}^{N}\chi(y_l - x_j^{k+1}) \\ &+ \frac{1}{2}e^{\kappa k\Delta t}\sum_{j=1}^{N}\chi(y_l - x_j^k)\end{aligned} \tag{32}$$

The coupling between the particle dynamics and the chemotaxis equation is realized by means of the gradient of φ, evaluated, at each time instant t_k, in the position of agent i at that time. The values of the gradient at grid points is approximated with centered difference, i.e. $\partial_l\varphi^k \approx \frac{\varphi_{l+1}^k - \varphi_{l-1}^k}{2\Delta x}$. Since x_i^k does not necessarely correspond to one of the grid point y_l, we approximate $\partial_x\varphi^s$ at time t_k with a linear interpolation of the values of the gradient at the nearest grid points, in the following denoted as $\Phi_{x_i^k}(\partial_l\varphi^k)$.

Recalling the choice of γ performed in (10), the numerical scheme implemented for (P) reads

$$\begin{cases} v_i^{k+1} = v_i^k + \frac{\Delta t}{N}\sum_{j=1}^{N}\frac{v_j^{k+1} - v_i^{k+1}}{\left(1 + \left\|x_i^k - x_j^k\right\|^2\right)^\beta} + \eta\Delta t\Phi_{x_i^k}(\partial_l\varphi^k) \\ x_i^{k+1} = x_i^k + \Delta t v_i^{k+1} \\ \varphi_l^k = e^{-\kappa k\Delta t}u_l^k \quad \text{with} \quad u_l^k \ \text{ approximated as in (32)} \end{cases} \tag{33}$$

Kinetic level: numerical scheme for (V)

Let now focus on system (V). The computational domain $\Omega \times [0, T]$ is divided in cells of side $\Delta x \times \Delta v \times \Delta t$ where Δx, Δv, are the space and velocity steps and Δt is the time step. Let us assume that T is a multiple of Δt to avoid rounding.

We choose Ω as a rectangular domain of size $n_x\Delta x \times n_v\Delta v$, with $n_x, n_v \in \mathbb{N}$ the number of inner point discretizing the space and velocity domain. The generic point of the 2-dimensional grid is hence denoted as (x_i, v_j) with $i = 0, ..., n_x$, $j = 0, ..., n_v$. We

consider periodic boundary condition with respect to the x variable, and null condition with respect to the v variable. For any time instant t_k we denote the approximation of ρ and ν at (x_i, v_j) with $\rho_{i,j}^k$ and $\mathcal{V}_{i,j}^k$, respectively. The first-order upwind scheme implemented reads:

$$\begin{aligned}\frac{\rho_{i,j}^{k+1}-\rho_{i,j}^k}{\Delta t} &= -\frac{v_j}{2\Delta x}\left(\rho_{i+1,j}^k-\rho_{i-1,j}^k\right)+\frac{|v_j|}{2\Delta x}\left(\rho_{i+1,j}^k-2\rho_{i,j}^k+\rho_{i-1,j}^k\right)\\ &-\frac{1}{2\Delta v}\left(\rho_{i+1,j}^k\mathcal{V}_{i+1,j}^k-\rho_{i-1,j}^k\mathcal{V}_{i-1,j}^k\right)\\ &+\frac{1}{2\Delta v}\left(\rho_{i+1,j}^k\left|\mathcal{V}_{i+1,j}^k\right|-2\rho_{i,j}^k\left|\mathcal{V}_{i,j}^k\right|+\rho_{i-1,j}^k\left|\mathcal{V}_{i-1,j}^k\right|\right).\end{aligned} \tag{34}$$

At each time step, a CFL condition of the form

$$1-\frac{\Delta t}{\Delta x}|v_{max}|-\frac{\Delta t}{\Delta v}\max_{i,j}\mathcal{V}_{i,j}^k\geq 0 \tag{35}$$

must be satisfied.

As at particle level, we approximate the solution of the chemotaxis equation by means of a second order centered finite differences method in space and a classical explicit-implicit Crank-Nicholson integration in time. The only difference is given by the source term. We approximate the two-dimensional integral in (17) using a rectangular quadrature formula. In greater details, it holds:

$$\int_{\mathbb{R}}\int_{x-R}^{x+R}\rho^s(y)dyd\xi\approx\sum_{\substack{m,n:\\ x_m\in[x_i-R\Delta x,x_i+R\Delta x],\\ n=0,\dots,n_v}}\rho_{m,n}^k\Delta x\Delta v$$

Concerning the coupling through the gradient, the approximation of $\partial_x\psi$ is required at spatial grid point. We approximate its value at each time instant using centered finite difference $\partial_i\psi^k\approx\frac{\psi_{i+1}^k-\psi_{i-1}^k}{2\Delta x}$.

Macroscopic level: numerical scheme for (E)

We describe the numerical scheme for the most general Euler system. The scheme used for system (20) and (23) can be obtained simply considering $\varepsilon=0,\eta=0,\alpha=0$ and $\varepsilon=0$, respectively.

Denoting $W=W(x,t)=(\mu^t(x),\mu^t(x)u^t(x))^T$ the vector of unknowns, density and momentum, we rewrite the hyperbolic part as

$$W_t+A(W)_x=S(W), \tag{36}$$

where A and S are defined as follow:

$$A(W)=\begin{pmatrix}\mu u\\ \mu u^2+\varepsilon P(\mu)\end{pmatrix}$$

$$S(W) = \begin{pmatrix} 0 \\ \mu \int \gamma(\cdot - y, u(\cdot) - u(y))\mu(y)dy + \eta\mu\partial_x\psi - \alpha\mu u \end{pmatrix}$$

We approximate the solution at each time step starting from the relaxation tecniques originally proposed in [**?**] In few words, the idea is to approximate hyperbolic system of equations through a BGK relaxation, which leads to a linear advection system with a relaxation source term. The advantage lies in the fact that at each time step t^k, in order to find the solution at t^{k+1}, it is required to solve a system of linear, transport problems, which reduces the computational complexity.

We denote with $X \subset \mathbb{R}$ the computational domain. We approximate the solution of Euler system $W_i^k = (\mu_i^k, \mu_i^k u_i^k)^T$ and of the parabolic equation ψ_i^k at each point of the grid $x_i = i\Delta x$, $i = 1, ..., n_x - 1$. At boundary, we assume $W_0 = W_{n_x} = (0, 0)^T$ The parabolic equation is approximated using the classical explicit-implicit Crank-Nicholson method, as previously explained. The algorithm requires to first solve a homogeneous system of equations and then a time integration of the source part is performed. Let now focus on the homogeneous part of (36). Using BGK approximation with two velocities of equal speed and opposite sign, i.e. $\lambda_1 = \lambda = -\lambda_2$ we denote with $\mathbf{f}_r = (f_r^\mu, f_r^{\mu u})$, $r = 1, 2$, the components of BGK model approximating W. For a complete description of the relaxation technique see [**?**]. At each time iteration we solve

$$\partial_t \begin{pmatrix} \mathbf{f}_1 \\ \mathbf{f}_2 \end{pmatrix} + \begin{pmatrix} \lambda & 0 & 0 & 0 \\ 0 & \lambda & 0 & 0 \\ 0 & 0 & -\lambda & 0 \\ 0 & 0 & 0 & -\lambda \end{pmatrix} \partial_x \begin{pmatrix} \mathbf{f}_1 \\ \mathbf{f}_2 \end{pmatrix} = \mathbf{0} \tag{37}$$

with initial states given by the Maxwellian functions

$$\begin{pmatrix} \mathbf{f}_1^0 \\ \mathbf{f}_2^0 \end{pmatrix} = \begin{pmatrix} \frac{1}{2}\left(W(x,0) + \frac{A(W(x,0))}{\lambda}\right) \\ \frac{1}{2}\left(W(x,0) - \frac{A(W(x,0))}{\lambda}\right) \end{pmatrix}$$

Denoting with $(\mathbf{f}_r)_i^k$, the approximated value of $\mathbf{f}_r$, at time t_k at grid point x_i, we compute $(\mathbf{f}_r)_i^{k+1/2}$ running the following numerical upwind scheme:

$$(\mathbf{f}_r)_i^{k+1/2} = (\mathbf{f}_r)_i^k - \frac{\Delta t}{2\Delta x}\lambda_r^k \left((\mathbf{f}_r)_{i+1}^k - (\mathbf{f}_r)_{i-1}^k\right) + \frac{\Delta t}{2\Delta x}|\lambda_r^k| \left((\mathbf{f}_r)_{i+1}^k - 2(\mathbf{f}_r)_i^k + (\mathbf{f}_r)_{i-1}^k\right)$$

for any $i = 1, ..., n_x$, $r = 1, 2$, with $\lambda_1^k = \max_i \left(|u_i^k| + \sqrt{P'(\mu_i^k)}\right)$, $\lambda_2^k = -\lambda_1^k$. The stability of the scheme is guaranteed choosing, at each time step, $\Delta t^k = 0.9\frac{\Delta x}{\lambda_1^k}$.

The solution W at time t_{k+1} is obtained adding the discretization of the source term $S(W)$. The integral term and the chemotaxis gradient are treated explicitly, whereas the damping term in implicit, due to stiffness problem. The approximated value of the integral term, in the following denoted as $\mathcal{I}_i^k$, is obtained by a first-order quadrature

formula, which has to be solved at each iteration. Finally we get

$$W_i^{k+1} = (\mathbf{f}_1)_i^{k+1/2} + (\mathbf{f}_2)_i^{k+1/2} + \Delta t \left(0, \mu_i^k \mathcal{I}_i^k + \eta \mu_i^k \frac{\psi_{i+1}^k - \psi_{i-1}^k}{2\Delta x}\right)$$

References

[1] G. Albi, and L. Pareschi. Binary interaction algorithms for the simulation of flocking and swarming dynamics. Multiscale Modeling and Simulation, 2013.

[2] D. Aregba-Driollet, and R. Natalini. Discrete kinetic schemes for multidimensional systems of conservation laws. SIAM Journal on Numerical Analysis 37.6 (2000): 1973-2004.

[3] Y. Arboleda-Estudillo, M. Krieg, J. Stühmer, N. A. Licata, D. J. Muller and C.-P. Heisenberg, Movement Directionality in Collective Migration of Germ Layer Progenitors, *Curr Biology*, **20** (2010) 161–169.

[4] J. M. Belmonte, G. L. Thomas, L. G. Brunnet, R. M. de Almeida and H. Chaté, Self-propelled particle model for cell-sorting phenomena, *Phys Rev Lett* **100** (2008) 248702.

[5] J. A. Carrillo, Y.-P. Choi, E. Tadmor, and C. Tan, Critical thresholds in 1D Euler equations with nonlocal forces, Math. Mod. Meth. Appl. Sci., 26:185–206 (2016).

[6] Carrillo, José A.; Choi, Young-Pil Mean-field limits: from particle descriptions to macroscopic equations. Arch. Ration. Mech. Anal. **24** (3) (2021) 1529-1573.

[7] J.A. Carrillo, M. Fonasier, G. Toscani, F. Vecil. Particle, kinetic, and hydrodynamic models of swarming Mathematical modeling of collective behavior in socio-economic and life sciences (pp. 297-336). Birkhäuser Boston. 2020.

[8] J.A. Carrillo, and F. Vecil. Nonoscillatory interpolation methods applied to Vlasov-based models. SIAM Journal on Scientific Computing 29.3 (2007): 1179-1206.

[9] Carrillo, José A., Young-Pil Choi, and Sergio P. Perez. A review on attractive–repulsive hydrodynamics for consensus in collective behavior. Active Particles, Volume 1: 259-298, 2017

[10] J. A. Carrillo, Y.-P. Choi, E. Tadmor, and C. Tan. Critical thresholds in 1D Euler equations with nonlocal forces. Math. Mod. Meth. Appl. Sci., 26:185-206, 2016.

[11] F. Cucker and S. Smale, On the mathematics of emergence. Japan. J. Math. **2** (2007) 197-227.

[12] F. Cucker and S. Smale, Emergent behavior in flocks. IEEE Trans. Automat. Control 52 (2007) 852-862.

[13] T. Colin, M.-C. Durrieu, J. Joie, Y. Lei, Y. Mammeri, C. Poignard and O. Saut, Modeling of the migration of endothelial cells on bioactive micropatterned polymers, *Math. BioSci. and Eng.*, **10** (2013) 997–1015.

[14] I. D. Couzin, J. Krause, N. R. Franks and S. A. Levin, Effective leadership and decision-making in animal groups on the move, *Nature*, **433** (2005) 513–516.

[15] M. R. D'Orsogna, Y. L. Chuang, A. L. Bertozzi and L. S. Chayes, Self-Propelled Particles with Soft-Core Interactions: Patterns, Stability, and Collapse, *Phys Rev Lett*, **96** (2006) 104302.

[16] E. Di Costanzo, R. Natalini, Roberto, L. Preziosi, A hybrid mathematical model for self-organizing cell migration in the zebrafish lateral line. J. Math. Biol. **71** (1) (2015) 171-214.

[17] E. Di Costanzo, M. Menci, E. Messina, R. Natalini, A. Vecchio, A hybrid model of collective motion of discrete particles under alignment and continuum chemotaxis, Discrete Contin. Dyn. Syst., Ser. B **25** (1) (2020) 443-472.

[18] A. Figalli and M.-J. Kang, A rigorous derivation from the kinetic Cucker-Smale model to the pressureless Euler system with nonlocal alignment, Anal. PDE. **12** (2019) 843–866.

[19] P. Haas P, D. Gilmour, Chemokine signaling mediates self-organizing tissue migration in the zebrafish lateral line. Dev Cell **10** (2006) 673–680.

[20] S.-Y. Ha, J. Kim, X. Zhang, Uniform stability of the Cucker-Smale model and applications to the mean-field limit, Kinetic and Related Models **11** (2018) 1157-1181

[21] S.-Y. Ha and J.-G. Liu, A simple proof of Cucker-Smale flocking dynamics and mean-field limit, Commun. Math. Sci. **7** (2009) 297-325.

[22] H. Hatzikirou and A. Deutsch, Collective guidance of collective cell migration, *Curr. Top. Dev. Biol.* **81** (2007) 401–434.

[23] P.-E. Jabin and Z. Wang, Mean Field limit and propagation of chaos for Vlasov systems with bounded forces, J. Funct. Anal. **271** (2016) 3588-3627.

[24] P.-E. Jabin and Z. Wang, Quantitative estimates of propagation of chaos for stochastic systems with $W-1,\infty$ kernels, Invent. Math. **214** (2018) 523-591.

[25] Lecaudey V, Akdogan GC, Norton WHJ, Gilmour D Dynamic Fgf signaling couples morphogenesis and migration in the zebrafish lateral line primordium. Development **135** (2008) 2695–2705.

[26] J. Joie, Y. Lei, M.-C. Durrieu, T. Colin, C. Poignard and O. Saut, Migration and orientation of endothelial cells on micropatterned polymers: a simple model based on classical mechanics, *Discrete Contin. Dyn. Syst. Ser. B* **20** (2015), 1059–1076.

[27] D. Kawashima, PhD Thesis, Kyoto University (1983).

[28] E. Méhes and T. Vicsek, Collective motion of cells: from experiments to models, *Integr Biol* **6** (2014) 831–854.

[29] M. Menci, M. Papi, Global solutions for a path-dependent hybrid system of differential equations under parabolic signal, Nonlinear Analysis **184** (2019) 172–192.

[30] M. Menci, M. Papi. Existence of solutions for hybrid systems of differential equations under exogenous information with discontinuous source term. Nonlinear Analysis **221** (2022): 112885.

[31] R. Natalini, T. Paul, On The Mean Field limit for Cucker-Smale models, Discrete & Continuous Dynamical Systems - B, doi: 10.3934/dcdsb.2021164.

[32] R. Natalini, T. Paul, The Mean-Field limit for hybrid models of collective motions with chemotaxis, to appear in SIAM Journal on Mathematical Analysis, hal-03310547.

[33] B. Piccoli, F. Rossi, E. Trélat, Control to flocking of the kinetic Cucker-Smale model, SIAM J. Math. Anal **47** (2014) 4685–4719.

[34] Preziosi, L.; Astanin, S. Modelling the formation of capillaries. Quarteroni, Alfio (ed.) et al., Complex systems in biomedicine. Milano: Springer 109-145, 2006.

[35] A. Colombi, M. Scianna and A. Tosin, Differentiated cell behavior: a multiscale approach using measure theory, *J Math Biol*, **71**(5) (2015) 1049-1079.

[36] N. Sepúlveda, L. Petitjean, O. Cochet, E. Grasland-Mongrain, P. Silberzan and V. Hakim, Collective Cell Motion in an Epithelial Sheet Can Be Quantitatively Described by a Stochastic Interacting Particle Model, *PLOS Computational Biology*, **9** (3) (2013) e1002944.
[37] D. Strömbom, Collective motion from local attraction, *J Theor Biol* **283** (2011) 145–151.
[38] B. Szabò, G. J. Szöllösi, B. Gönci, Z. Jurànyi, D. Selmeczi and T. Vicsek, Phase transition in the collective migration of tissue cells: Experiment and model, *Phys Rev E* **74** (2006) 061908.
[39] A.-S. Sznitman, Topics in propagation of chaos. Ecole d'Et´e de Probabilit´es de Saint-Flour XIX, Lecture Notes in Math. 1464. Springer-Verlag, Berlin, 1991.
[40] E. Tadmor, Swarming: hydrodynamic alignment with pressure. arXiv preprint arXiv:2208.11786
[41] T. Vicsek, A. Cziròk, E. Ben-Jacob, I. Cohen and O. Shochet, Novel Type of Phase Transition in a System of Self-Driven Particles, *Phys Rev Lett*, **75** (1995) 1226–1229.
[42] T. Vicsek and A. Zafeiris, Collective motion, *Physics Reports* **517** (2012),71–140.
[43] C. Villani: Topics in Optimal Transportation, Amer. Math. Soc., Providence (RI), 2003.
[44] C. Villani: Optimal Transport. Old and New, Springer-Verlag, Berlin, Heidelberg, 2009.

(M.M) Università Campus Bio-Medico di Roma Via Àlvaro del Portillo 00128 Roma, Italy
Email address: m.menci@unicampus.it

(R.N) IAC, Via dei Taurini, 19, 00185 Roma RM Italy
Email address: roberto.natalini@cnr.it

(T.P.) CNRS Laboratoire Ypatia des Sciences Mathématiques (LYSM), Roma, Italia & Sorbonne Université, CNRS, Université Paris Cité, Laboratoire Jacques-Louis Lions (LJLL), F-75005 Paris, France
Email address: thierry.paul@sorbonne-universite.fr